Applied Physics Letters

Solid and hollow metallic glass microneedles for transdermal drug-delivery

Cite as: Appl. Phys. Lett. **116**, 203703 (2020); https://doi.org/10.1063/5.0008983
Submitted: 26 March 2020 . Accepted: 06 May 2020 . Published Online: 19 May 2020

Zhonglue Hu, Chandra S. Meduri, Rohan S. J. Ingrole, Harvinder S. Gill, and Golden Kumar

Applied Physics Letters ARTICLE scitation.org/journal/apl

Solid and hollow metallic glass microneedles for transdermal drug-delivery

Cite as: Appl. Phys. Lett. **116**, 203703 (2020); doi: 10.1063/5.0008983
Submitted: 26 March 2020 · Accepted: 6 May 2020 ·
Published Online: 19 May 2020

Zhonglue Hu,[1,2] Chandra S. Meduri,[2] Rohan S. J. Ingrole,[3] Harvinder S. Gill,[3,a)] and Golden Kumar[2,b)]

AFFILIATIONS

[1]College of Engineering, Zhejiang Normal University, Jinhua 321004, China
[2]Department of Mechanical Engineering, The University of Texas at Dallas, Richardson, Texas 75080, USA
[3]Department of Chemical Engineering, Texas Tech University, Lubbock, Texas 79409, USA

[a)]**Email:** Harvinder.Gill@ttu.edu
[b)]**Author to whom correspondence should be addressed:** Golden.Kumar@UTDallas.edu

ABSTRACT

Metallic microneedles are attractive for painless transdermal drug-delivery. However, fabrication techniques for metal microneedles are often complex and multi-step. In this study, a scalable manufacturing of metallic microneedle arrays is presented using thermoplastic drawing of metallic glasses. Microneedles with tunable lengths and tips are produced by controlling the rheology and fracture of metallic glass. The same drawing process can generate solid and hollow microneedles simply by varying the thickness of metallic glass. The mechanism of thickness dependent transition from solid to hollow profiles is described by the viscous buckling of metallic liquid. *In vitro* skin insertion tests demonstrate that both solid and hollow metallic glass microneedles can pierce porcine skin and deliver model drugs.

Microneedles are extensively studied for biomedical applications such as, transdermal drug-delivery,[1,2] oral cavity drug-delivery,[3] and sensing.[4] Microneedles offer a minimally invasive and painless delivery method and have been widely investigated for the delivery of pharmaceuticals[5] and vaccines.[6] With increasing momentum in the field, clinical translation of microneedle technology demands a scalable and cost-effective method of microneedle fabrication. Numerous techniques such as laser cutting,[7] micromolding,[8] micromachining,[9] and fiber drawing[10] have been used to produce microneedles from polymers, semiconductors, ceramics, and metals. By piercing through the skin's outmost layer, the stratum corneum, solid microneedles can increase the skin permeability for subsequent topical treatment or can be directly coated with drugs, whereas hollow microneedles can deliver the drugs through controlled pressure-driven flow.[2,11]

The shape and size of microneedles are critical to enable penetration of stratum corneum without causing pain. Shapes such as, bevel, chisel, and tapered cones with small radii of curvatures are preferred for microneedle tips to reduce the force of insertion.[2,7] Optimal lengths of microneedles are also critical to prevent buckling failure and undesired pain from deep penetration.[2,7] In addition, the microneedles should be made from a biocompatible material. Metals are ideal candidates for microneedles because of their high resistance to buckling and fracture. While polymer microneedles can be produced through high-throughput thermoplastic or soft lithography methods, metal microneedles require multiple processing steps. Two main approaches used in the fabrication of metal microneedles are laser cutting and electrodeposition.[7] The laser based technique involves cutting of needle shapes in a thin metal sheet followed by out-of-plane bending of each needle in a sequential manner.[7] Hollow metal microneedles have been possible only by metal deposition on sacrificial polymer structures. This requires fabrication of polymer microneedles, coating of the metal layer, and selective etching of the polymer core.[12] Therefore, there is a need for a simple and high-throughput manufacturing technique for metal microneedles for transdermal drug-delivery and other applications that require conductive microelectrodes.

One potential solution is to advance different metallic materials that are amenable to non-lithographic fabrication methods. Metallic glasses (MGs) are one such class of metals, which exhibit many physical and chemical properties like conventional metals but can be thermoplastically molded like polymers.[13] The mechanical properties of MGs such as, high Young's modulus and yield strength, and good wear resistance are ideally suited for applications as blades, scalpels, and needles.[14] It has been shown that MG coatings can significantly reduce the friction and insertion force of hypodermic needles due to

the smooth surface and lack of crystal defects in MGs.[15,16] Previous studies have also indicated that several MGs exhibit good biocompatibility, antibacterial property, and biodegradability.[17–20] The combination of chemical, mechanical, and thermoplastic properties has increased interest in MGs for biomedical applications.[15–23] In this study, we demonstrate the fabrication of microneedles using thermoplastic drawing of Pt-based MG ($Pt_{57.5}Cu_{14.7}Ni_{5.3}P_{22.5}$) for transdermal drug-delivery applications. The results show that arrays of metallic microneedles with controllable lengths, tip shapes, and profiles (solid or hollow) can be fabricated by simple thermomechanical processing.

Figure 1 illustrates the thermoplastic drawing scheme used for the fabrication of MG microneedles with different tip shapes. An aluminum (Al) template with a cylindrical cavity was attached to a heating plate mounted on a mechanical testing machine. A cavity diameter of 200 μm and a length of 1 mm were selected to fabricate microneedles suitable for transdermal applications. Two heating plates were heated to 270 °C, to ensure that the MG has a low viscosity (10^5–10^9 Pa.s) but a sufficiently long crystallization time (>5 min). A piece of Pt-based MG was pressed between the template and a movable upper heating plate that was polished to ensure strong adhesion with the MG [Fig. 1(a)]. The viscous MG filled the template cavity under an applied pressure of about 10 MPa. Subsequently, the MG microneedle was drawn from the cavity by pulling the top plate upward [Fig. 1(b)]. Three distinct tip shapes were produced by varying the pulling speed (strain-rate). Similar shapes could be achieved by varying the processing temperature (viscosity) at a fixed pulling speed. At a slow pulling speed (or high temperature), the MG fiber necks and separates into two conical microneedles; one attached to the template and the other to the MG [Fig. 1(c)]. At an intermediate pulling speed, gradual thinning of MG results in drawing of relatively uniform fiber [Fig. 1(d)]. The drawing can be stopped after achieving a desirable fiber length and bevel shaped microneedles are created by subsequent fracture at room temperature. Further increase in the pulling speed causes demolding of MG from the cavity and the tip retains a parabolic shape formed during pressing [Fig. 1(e)]. The SEM images also demonstrate the feasibility of drawing from multiple cavities for the fabrication of microneedle arrays (Fig. 1). Similar tip shapes (conical, bevel, and parabolic) as in the single microneedle are achieved in the arrays.

The shape of thermoplastically drawn MG is governed by an interplay between the viscous stress, the capillary stress, and the adhesive strength.[24,25] The length (L) and the tip diameter (D) of the drawn MG microneedle can be predicted for all three different tip types (conical, bevel, and parabolic). For conical tips formed by necking (at slow pulling speed or high temperature), the capillary stress exceeds the viscous stress and the tip diameter evolves as[25]

$$D = D_0\left(\frac{\pi D_0}{\alpha L_e + 2D_0}\right)\left(1 - \frac{L_e}{L_B}\right), \tag{1}$$

where D_o is the initial diameter of MG (same as the cavity diameter), L_e is the extensional displacement of the top plate, L_B is the theoretical length of the MG fiber at breakup (when D approaches zero), and α is a fitting parameter related to the initial conditions. The length of the viscous fiber at breakup due to surface tension can be estimated as[26]

$$L_B = \left(\frac{3v\eta D_0}{\gamma}\right) \tag{2}$$

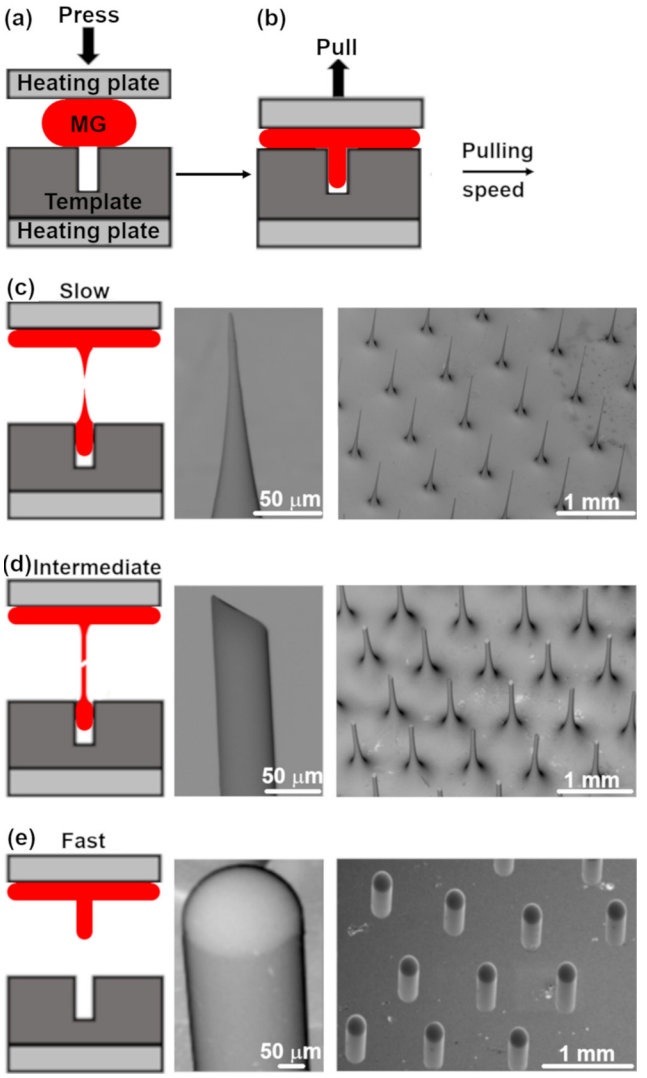

FIG. 1. Fabrication of microneedles using thermoplastic drawing of Pt-based MG. (a) MG is heated and embossed into a template cavity. (b) MG fiber is drawn from the cavity at different speeds while keeping the temperature constant. (c) MG fiber necks and breaks into conical microneedles at a slow pulling speed. (d) A nearly uniform MG fiber is drawn at an intermediate speed, which is fractured at room temperature to create bevel shaped microneedles. (e) At a fast pulling speed, the MG separates from the cavity resulting in the formation of the parabolic tip profile.

where v is the pulling speed, η is the MG viscosity, and γ is the surface tension of MG. A desirable combination of D and L ($\approx L_e/2$) for conical microneedles can be achieved by tuning the L_B through variation in viscosity and drawing speed [Eq. (2)]. Uniform MG microneedles with bevel shaped tips can be generated by increasing the pulling speed or lowering the temperature. Under these conditions, the viscous stress dominates and the capillary term in Eq. (1) can be ignored to yield

$$D = D_0\left(\frac{\pi D_0}{\alpha L_e + 2D_0}\right). \tag{3}$$

In order to independently control D and L_e in Eq. (3), the volume of MG subjected to elongation can be varied by changing the initial conditions.[25] The uniformly drawn MG fiber can be fractured into microneedles of desirable lengths with bevel shaped tips at room temperature. Shear-localized tensile failure of MG inherently creates bevel shapes with a fracture angle of 50–60°.[14] At a very fast pulling speed or low temperature, the flow stress of MG exceeds its adhesive strength and it demolds from the cavity. The length and diameter of the demolded MG remain essentially the same as achieved during molding, which are precisely controllable.[13,27]

The theoretical predictions [Eqs. (1) and (3)] are also applicable to drawing of multiple MG microneedles. For example, the lengths of microneedles calculated from Eq. (3) are compared with the measured lengths of arrays of 50 microneedles (supplementary material Fig. S1). Less than 10% deviation from the predicted lengths is observed which is primarily due to use of approximate values of viscosity and surface tension in equations. These findings demonstrate that thermoplastic drawing of MGs is a facile manufacturing technique for metallic microneedle arrays with different lengths and tip shapes.

MG microneedle arrays were tested *in vitro* for transdermal drug-delivery applications using porcine skin. All three types of MG microneedles (shown in Fig. 1) were able to penetrate the skin without failure but the drug-delivery tests were conducted on demolded microneedles because of their uniform lengths. MG microneedles were loaded with different drug formulations using dip-coating [Fig. 2(a)]. A patch of 21 Pt-based MG microneedles (length ~ 656 μm and diameter ~ 200 μm) was dipped into an aqueous reservoir of drug solution. As shown in Fig. 2(d), the fluorescent sulforhodamine solution could be coated on the MG microneedles. A closer view of a single microneedle [Fig. 2(e)] shows that the dye was mainly coated on the microneedle and the contamination of base MG was minimal. This observation is further supported by the corresponding fluorescent image [Fig. 2(f)] where the red color is observed only on the microneedle surface. Other formulations such as riboflavin [Fig. 2(g)] and micro-particle solution [Fig. 2(h)] were also coated on the MG microneedles using the dip-coating approach.

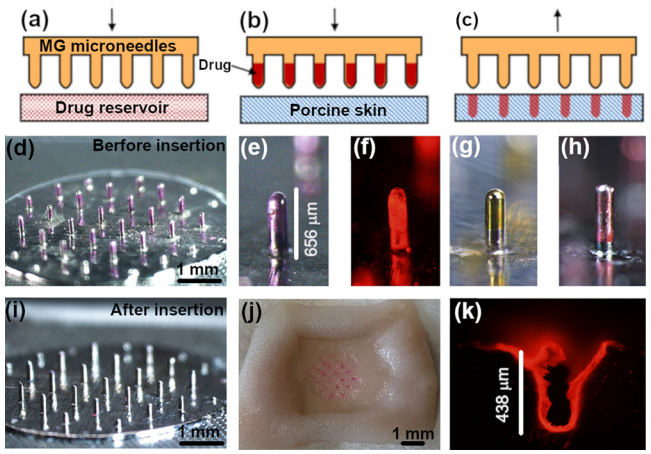

FIG. 2. Transdermal drug-delivery using Pt-based MG microneedle arrays. Schematic illustrations of (a) coating, (b) insertion, and (c) removal of microneedles. (d) Brightfield micrograph of Pt-based MG microneedles coated with fluorescent sulforhodamine dye. (e) Enlarged view of a single microneedle and (f) the corresponding fluorescent image. Brightfield images of MG microneedles coated with (g) riboflavin and (h) polystyrene/divinylbenzene microparticles. (i) MG microneedles after delivering coated sulforhodamine into porcine cadaver skin and (j) the image of the corresponding area of porcine cadaver skin. (k) Fluorescent image of the histological section of the porcine cadaver skin after inserting the microneedle coated with sulforhodamine.

To determine if the coated drug can be delivered into the skin, the patch of coated MG microneedles was inserted into porcine cadaver skin [Fig. 2(b)] and was removed after 3 min [Fig. 2(c)]. The microneedles regained their metallic luster upon removal from the skin [Fig. 2(i)] indicating that the coated drug had been removed from the microneedles. Red spots corresponding to the insertion points are clearly visible on the porcine skin [Fig. 2(j)] due to the transfer of fluorescent dye from the microneedles. Further histological examination reveals that the insertion of MG microneedles created 430–450 μm long channels in the dermis layer [Fig. 2(k)]. The fluorescent layer observed along the inner surface of the microchannels confirms the delivery of the drug in the skin. No significant contamination of the drug on the surface of skin was detected. These results demonstrate that MG solid microneedles can be used for transdermal drug-delivery applications.

Thermoplastic drawing of MGs can also produce hollow microneedles using the same press-and-pull process as used for the solid microneedles. We recently reported that the thermoplastic pressing of thin MG against a template cavity creates a buckle (dimple) on the backside of MG.[24] Such thickness dependent buckling can be harnessed in tailoring the profile (hollow or solid) of drawn MG microneedles (Fig. 3). The thickness of MG decreases during thermoplastic pressing due to lateral and vertical flows.[28,29] If the thickness drops below half of the cavity diameter, the viscous liquid buckles under compression [Figs. 3(a) and 3(b)]. The buckling creates localized delamination of MG from the top heating plate. The gap created between the MG and the heating plate acts as a seed for the formation

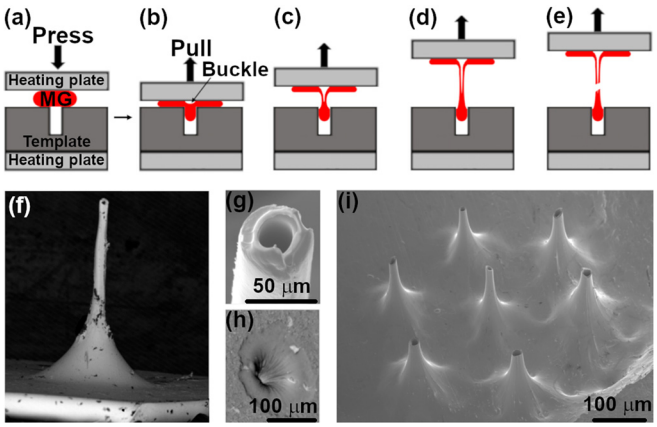

FIG. 3. Fabrication of hollow MG microneedles. (a) A small volume of MG is thermoplastically pressed against a template cavity. (b) The MG becomes thin and delaminates from the top plate due to viscous buckling. (c) and (d) The buckle elongates into a long hollow MG tube during drawing. (e) The MG tube is fractured to create an open hollow microneedle attached to the top plate. (f) Single hollow microneedle drawn from Pt-based MG. The top (g) and bottom (h) ends of the MG microneedle. (i) An array of six hollow Pt-based MG microneedles made by drawing.

of a hollow conduit during subsequent drawing [Figs. 3(c) and 3(d)]. Room temperature fracture of hollow conduit creates an open-ended metallic microneedle [Fig. 3(e)]. Figure 3(f) shows a hollow microneedle drawn under the same conditions as the solid microneedle but using a thinner Pt-based MG (thickness ~100 μm). The SEM images of the top [Fig. 3(g)] and the base [Fig. 3(h)] of the microneedle reveal the formation of a through hole. Furthermore, multiple hollow microneedles can also be drawn using multiple cavities as shown in Fig. 3(i).

The evolution of hole formation during drawing was investigated by systematically varying the thickness of MG (supplementary material Fig. S2). The results clearly demonstrate that hollow and solid MG microneedles can be fabricated by the same drawing process by using MGs of different thicknesses. Hollow MG microneedles were tested for the injection of fluid into porcine skin. A Pt-based MG hollow microneedle with an opening of about 80 μm was mounted onto a 1 ml syringe using a custom-made cap [Fig. 4(a)]. One end of the cap contained a conical bore to enable tight fitting to the syringe and the other end had a cylindrical opening (diameter ~1 mm) to house the hollow microneedle [Fig. 4(b)]. The microneedle was glued to the cap and about 500 μm long shaft was exposed from the cap opening [Fig. 4(c)]. As shown in the image sequence [Figs. 4(d) and 4(f)], a water jet can be injected through the orifice of the MG microneedle upon applying a small pressure. Using this MG hollow microneedle, we injected about 100 μL of sulforhodamine solution to the porcine cadaver skin with minimal backflow. Figures 4(g) and 4(h) compares the brightfield images of the porcine skin before and after injection. The color contrast shows the delivery of sulforhodamine to the skin. This finding was further validated by the corresponding fluorescent image [Fig. 4(i)], where the illuminated area marks the presence of the fluorescent dye. The larger illuminated area in the fluorescent image is an indicator of lateral and vertical diffusion of the injected dye. These observations provide a clear evidence that the sulforhodamine solution was effectively injected using the MG hollow microneedle.

In summary, we demonstrated thermoplastic drawing of MGs for the fabrication of microneedles for transdermal drug-delivery applications. Arrays of microneedles with controllable lengths and tip shapes were produced by varying the drawing speed. A buckling assisted drawing scheme was developed to create hollow MG microneedles. The hollow and solid MG microneedles can be drawn using the same hardware and experimental conditions, merely by changing the thickness of MG. Solid microneedles were effectively coated with different solutions and inserted into porcine cadaver skin without mechanical failure. The skin examination after removing the microneedles revealed that coatings were effectively deposited in the epidermis layer. Injection of fluid into the skin was also demonstrated using a hollow MG microneedle.

High strength and elasticity, low friction, chemical homogeneity, and biocompatibility of MGs are ideal traits for biomedical devices. The cost and ductility limitations of MGs are alleviated in microneedle applications because of less material requirement and constrained loading. Recent advancements in thermoplastic forming of MGs such as, sheet making, and fiber drawing can enable manufacturing of large microneedle arrays. Our findings provide a proof-of-concept but quantitative studies on biocompatibility, drug loading, and delivery rates of MG microneedles are required to advance the use of MGs in transdermal applications. Drawing of hollow MG microneedles will be of particular interest to the microneedle community because the existing techniques for the fabrication of hollow metallic microneedles require multiple complex steps. Arrays of long MG fibers can also be potentially used as neural electrodes, which currently rely on extensive use of lithography.

See the supplementary material for the description of the experimental details of metallic glass synthesis, fabrication of solid and microneedles, drug-coating procedure, and skin insertion tests.

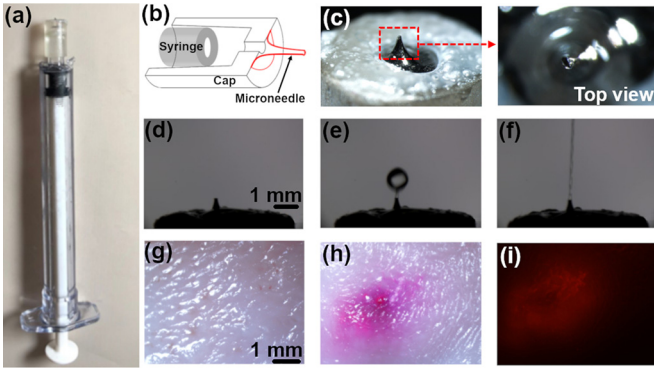

FIG. 4. *In vitro* testing of the Pt-based MG hollow microneedle. (a) MG hollow microneedle mounted on a 1 ml syringe using a custom-made cap. (b) Cross-sectional depiction of the cap assembly. (c) MG microneedle protruding from the cap and the magnified top view of the microneedle. (d)–(f) Image sequence of water jet ejected through the hollow MG microneedle. Brightfield images of porcine cadaver skin (g) before injection and (h) after injecting sulforhodamine using the MG hollow microneedle. (i) Fluorescent image of the injected area.

This work was supported by the National Science Foundation (NSF) through CMMI Award No. #1919445 and NSF-CAREER Award No.#1921435 awarded to GK, and by the National Institute of Allergy and Infectious Diseases of the National Institutes of Health under Award Nos. # R01AI135197 and # R01AI121322 to HSG.

DATA AVAILABILITY

The data that support the findings of this study are available from the corresponding author upon reasonable request.

REFERENCES

[1]R. S. J. Ingrole and H. S. Gill, J. Pharmacol. Exp. Ther. **370**, 555 (2019).
[2]M. R. Prausnitz, Ann. Rev. Chem. Biomol. Eng. **8**, 177 (2017).
[3]Y. Ma, W. Tao, S. J. Krebs, W. F. Sutton, N. L. Haigwood, and H. S. Gill, Pharm. Res. **31**, 2393 (2014).
[4]D. Al Sulaiman, J. Y. H. Chang, N. R. Bennett, H. Topouzi, C. A. Higgins, D. J. Irvine, and S. Ladame, ACS Nano **13**, 9620 (2019).
[5]A. K. Jain, C. H. Lee, and H. S. Gill, J. Controlled Release **239**, 72 (2016).
[6]J. Arya and M. R. Prausnitz, J. Controlled Release **240**, 135 (2016).
[7]H. S. Gill and M. R. Prausnitz, J. Controlled Release **117**, 227 (2007).
[8]K. Tsioris, W. K. Raja, E. M. Pritchard, B. Panilaitis, D. L. Kaplan, and F. G. Omenetto, Adv. Funct. Mater. **22**, 330 (2012).
[9]E. R. Parker, M. P. Rao, K. L. Turner, C. D. Meinhart, and N. C. MacDonald, J. Microelectromech. Syst. **16**, 289 (2007).

[10]K. Lee, H. Lee, D. S. Lee, and H. Jung, Adv. Mater. **22**, 483 (2010).
[11]G. S. Liu, Y. Kong, Y. Wang, Y. Luo, X. Fan, X. Xie, B. R. Yang, and M. X. Wu, Biomaterials **232**, 119740 (2020).
[12]K. Lee and H. Jung, Biomaterials **33**, 7309 (2012).
[13]J. Schroers, JOM **57**, 35 (2005).
[14]C. A. Schuh, T. C. Hufnagel, and U. Ramamurty, Acta Mater. **55**, 4067 (2007).
[15]J. P. Chu, C. C. Yu, Y. Tanatsugu, M. Yasuzawa, and Y. L. Shen, Sci. Rep. **6**, 31847 (2016).
[16]J. P. Chu, N. Boenninghoff, C. C. Yu, Y. K. Liu, and G. H. Chiang, Thin Solid Films **688**, 137320 (2019).
[17]C. L. Qiu, Q. Chen, L. Liu, K. C. Chan, J. X. Zhou, P. P. Chen, and S. M. Zhang, Scr. Mater. **55**, 605 (2006).
[18]Z. Liu, L. Huang, W. Wu, X. Luo, M. Shi, P. K. Liaw, W. He, and T. Zhang, Non-Cryst. Solids **363**, 1 (2013).
[19]J. P. Chu, T. Y. Liu, C. L. Li, C. H. Wang, J. S. C. Jang, M. J. Chen, S. H. Chang, and W. C. Huang, Thin Solid Films **561**, 102 (2014).
[20]B. Zberg, P. J. Uggowitzer, and J. J. Loeffler, Nat. Mater. **8**, 887 (2009).
[21]P. Meagher, E. D. O'Cearbhaill, J. H. Byrne, and D. J. Browne, Adv. Mater. **28**, 5755 (2016).
[22]J. Schroers, G. Kumar, T. M. Hodges, S. Chan, and T. R. Kyriakides, JOM **61**, 21 (2009).
[23]M. Shayan, J. Padmanabhan, A. H. Morris, B. Cheung, R. Smith, J. Schroers, and T. R. Kyriakides, Acta Biomater. **75**, 427 (2018).
[24]M. Hasan and G. Kumar, Nanoscale **9**, 3261 (2017).
[25]Z. Hu, C. S. Meduri, J. Blawzdziewicz, and G. Kumar, Nanotechnology **30**, 075302 (2019).
[26]G. H. Mckinley and A. Tripathi, J. Rheol. **44**, 653 (2000).
[27]J. Schroers, Adv. Mater. **22**, 1566 (2010).
[28]C. S. Meduri, Z. Hu, J. Blawzdziewicz, and G. Kumar, Appl. Phys. Lett. **114**, 113102 (2019).
[29]G. Kumar, J. Blawzdziewicz, and J. Schroers, Nanotechnology **24**, 105301 (2013).